Materials Today Bio 16 (2022) 100404

Contents lists available at ScienceDirect

Materials Today Bio

journal homepage: www.journals.elsevier.com/materials-today-bio

Functional importance of coacervation to convert calcium polyphosphate nanoparticles into the physiologically active state

Werner E.G. Müller [a,*], Meik Neufurth [a], Ingo Lieberwirth [b], Shunfeng Wang [a], Heinz C. Schröder [a], Xiaohong Wang [a,**]

[a] ERC Advanced Investigator Grant Research Group at the Institute for Physiological Chemistry, University Medical Center of the Johannes Gutenberg University, Duesbergweg 6, D-55128, Mainz, Germany

[b] Max Planck Institute for Polymer Research, Ackermannweg 10, 55128, Mainz, Germany

ARTICLE INFO

Keywords:
Inorganic polyphosphate
Nanoparticles
Coacervate
Alkaline phosphatase
ATP

ABSTRACT

Inorganic polyphosphates (polyP) are of increasing medical interest due to their unprecedented ability to exhibit both morphogenetic and ATP-delivering properties. However, these polymers are only physiologically active in the coacervate state, but not as amorphous nanoparticles (NP), the storage form of the polymer. Little is known about the mechanism of formation and interconversion of these two distinct polyP phases in the presence of metal ions. Based on in silico simulation studies, showing a differential clustering of polyP and calcium ions, the pH-dependent NP and coacervate formation of polyP was examined experimentally. Turbidimetric studies showed that Ca-polyP coacervate formation at pH 7 is a slow process compared to NP formation at pH 10. In FTIR spectra, the asymmetric stretching vibration signal of the internal $(PO_2)^-$ units, which is present in the Ca-polyP coacervate formed at pH 7, disappears in the NP formed at pH 10 using the conventional method (dropping of a $CaCl_2$ solution into a Na-polyP solution). Surprisingly, when reversing the procedure, adding Na-polyP to $CaCl_2$, a coacervate is obtained at both pH 7 and pH 10, as confirmed by SEM and FTIR analyses. The $(PO_2)^-$ signal also disappears when Ca-polyP-NP are exposed to peptides, leading to the transformation of the NP into the coacervate phase. From these results, a mechanistic model of pH-dependent coacervate and NP formation is proposed that considers not only electrostatic ion-ion but also ion-dipole interactions. Functional studies revealed a delayed polyP release kinetics for Ca-polyP-NP embedded in a hydrogel due to NP/coacervate conversion. Human A549 epithelial cells grown on the coacervate show increased proliferation and ATP production compared to cells cultured on particulate polyP. Ca-polyP NP taken up by endocytosis undergo intracellular coacervate transformation. Understanding the differential expression of the two polyP phases is of functional importance for the potential therapeutic application of this physiological, regeneratively active polymer.

1. Introduction

The first precise visualization and documentation of particles around 100 nm came from R. A. Zsigmondy [1] using dark field ultramicroscopy; he coined the term "nanoparticles" for particles in the 10–100 nm range. Soon later, Langmuir [2] and Blodgett [3] introduced the concept of monolayer surface chemistry [4]. Nanoparticles (NP) occur as fine colloidal suspensions in the atmosphere, originating from volcanic eruptions or produced by human activities [5]. NP also exist physiologically, e.g. in blood platelets, consisting of polyphosphate (polyP) with an average size of 100–200 nm [6,7]. The formation of the polyP NP proceeds through polyP precipitation in the presence of divalent metal ions, especially Ca^{2+}. Prior to the present report, our group succeeded in preparing such polyP nanoparticles from Na-polyphosphate (Na-polyP)

Abbreviations: ADK, adenylate kinase; ALP, alkaline phosphatase; Ap_5A, (P^1,P^5-di(adenosine-5′)pentaphosphate; ATP, adenosine triphosphate; Ca-polyP-Coa, calcium polyphosphate coacervate; Ca-polyP-NP, calcium polyphosphate nanoparticles; ECM, extracellular matrix; FTIR, Fourier Transformed Infrared Spectroscopy; LEV, levamisole; Na-polyP, sodium polyphosphate; NP, nanoparticles; P_i, orthophosphate; polyP, polyphosphate; PVA, poly(vinyl alcohol); SEM, scanning electron microscopy; TEM, transmission electron microscopy.

* Corresponding author. ERC Advanced Investigator Grant Research Group at Institute for Physiological Chemistry, University Medical Center of the Johannes Gutenberg University, Duesbergweg 6, D-55128, Mainz, Germany.

** Corresponding author.

E-mail addresses: wmueller@uni-mainz.de (W.E.G. Müller), wang013@uni-mainz.de (X. Wang).

https://doi.org/10.1016/j.mtbio.2022.100404
Received 5 July 2022; Received in revised form 15 August 2022; Accepted 16 August 2022
Available online 21 August 2022

together with Ca^{2+} in a bioinspired way.

In most previous studies on polyP, the physico-chemical mechanism by which NP become functionally active has remained open. Going back to Bütschli [8], who introduced studies on colloidal dispersions from water-in-water emulsions [9], it was recognized that solid phases (as a precursor stage) must undergo a transition into an aqueous intermediate product that is biologically and functionally active. The resulting intermediate associates, which consist of amorphous, non-crystalline particles, are also referred to as coacervates [10]. The process of coacervation is based on the formation of polymer droplets in solution, driven by the separation into two liquid phases, a highly concentrated colloidal phase, the coacervate, and a highly dilute colloidal phase [11]. The two colloidal aqueous phases are immiscible and are in thermodynamic equilibrium. The reversible transition between an immiscible and a miscible colloidal system is mandatory for the functional activity of a coacervate. While large positive or negative zeta potentials (e.g., around +30 and −30 mV) of particles dispersed in solution cause repulsion, leading to stabilization of (bioinert) NP, low zeta potentials promote coacervate formation. This property is exploited by the polyP/Ca^{2+}-NP when added to a physiological environment. When these particles are transferred to a proteinaceous milieu, their zeta potential drops and transformation into the coacervate phase occurs [12]. The coacervate phase represents the biologically active form of polyP and similar potentially active molecules [12,13].

The relevance of coacervation as a physiological control mechanism between inert NP and functionally active coacervate is usually underestimated [12,14]. For the formation of the NP, a superstoichiometric ratio between Ca^{2+} and phosphate units ($[PO_3]^-$) of polyP [12] was chosen to ensure that the polyanionic polyP chains in the NP are surrounded by a net-positive Ca^{2+} surface. Such particles have been shown to be more readily taken up by human Caco-2 cells than those with a negative surface charge [15].

PolyP is a distinguished polymer that underscores the physiological relevance of a controlled transition between the NP state and the coacervate phase. This polymer is accumulated in the acidocalcisomes with an acidic milieu [16]. At the pH ~5 present there, phosphoric acid occur as $H_2PO_4^-$, which in turn forms a Ca^{2+} salt $Ca(H_2PO_4)_2$, which is readily soluble in water (18 g L^{-1}). At a pH around 7 (near the $pK_{a\text{-}2}$ of 7.09), ~50% of the phosphoric acid is present as $H_2PO_4^-$ and ~50% as HPO_4^{2-}, respectively. With increasing pH, the solubility of the Ca^{2+}-phosphate salts decreases rapidly and an almost insoluble salt $Ca_3(PO_4)_2$ (0.02 g L^{-1}) is formed [17]. In the acidocalcisomes, where polyP is stored, the phosphorus content (141 μg [in ~200 insect eggs]) far exceeds the Ca^{2+} content (18 μg), suggesting that in this acidic environment the phosphate deposits largely exist as polyP/Ca^{2+}-NP [18]. From the acidocalcisomes of the blood platelets, polyP is released into the extracellular space. The phosphate concentration there (1×10^{-3} M) is comparatively low compared to the intracellular concentration of 200×10^{-3} M [19]. Even the comparatively high intracellular Ca^{2+} level of 1 mM [20] does not favor the precipitation of the calcium salts of the monomeric phosphate under the existing pH conditions. Later under "Results" it is shown that at a pH ~7 aggregates of the calcium salts of polymeric phosphate (Ca-polyP) are formed that are in an aqueous coacervate phase, or at pH ~10 in the particulate NP state.

In general, it is obvious that the degree of solubility of Ca-phosphate/polyP salts/NP determines both the direction and the intensity of the downstream reactions. Therefore, to get an evidence-based view of the functional potential of Ca-polyP-NP in silico, modeling and simulation studies were performed with Ca^{2+} and polyP in an aqueous milieu. Based on our data reported here, a fairly straightforward vision could be derived revealing a pH-dependent sorting and clustering of Ca^{2+} in the polyP environment. Furthermore, elucidating the pH dependence of the NP/coacervate mechanism also provided additional understanding of the accessibility of this inorganic polymer in a biological environment. In the coacervate phase, the release of polyP is faster and more extensive compared to the kinetics of polymer release from the NP phase.

In the final series of experiments, it is documented that cells cultivated on the coacervate phase show a more intense proliferation and cell layer formation. As a functional consequence, the cells growing on the coacervate release considerably more ATP into the extracellular matrix (ECM) than cells cultured on particulate polyP (Ca-polyP-NP). The property of polyP to function as a storage form for metabolic energy is dependent on the enzymatic cleavage of polyP via the enzyme alkaline phosphatase (ALP) and the subsequent phosphotransferase enzyme, adenylate kinase (ADK), which catalyzes the reversible interconversion of the three adenosine phosphates (ATP, ADP, and AMP) [21].

The presented coacervate, a Newtonian fluid, with its biocompatible viscosity offers human epithelial A549 cells a suitable environment to spread and to develop their functional potential. These cells have been found to release ATP in a Ca^{2+}-dependent manner [22]. The data shown here also underscore the importance and necessity of the coacervate phase of Ca-polyP as a transition state of the biologically inert, stable storage form of polyP, the Ca-polyP nanoparticles, which enables the polymer to exhibit its energy-rich and growth-stimulatory properties.

2. Materials and Methods

2.1. Materials

Na-polyphosphate (Na-polyP) with an average chain length of 40 orthophosphate (P_i) units was purchased from Chemische Fabrik Budenheim (Budenheim; Germany).

2.2. Preparation of Ca-polyP-coacervate

The coacervate of Na-polyP was obtained by mixing an aqueous solutions of Na-polyP (100 mL of a 0.48 M solution; based on P_i) with $CaCl_2 \cdot 2H_2O$ (C3306, Sigma; 100 mL of a 1.2 M solution). Unless otherwise noted, the $CaCl_2$ solution was added to the polyP solution under vigorous mixing, using a magnetic stirrer at a rate of 5 mL min^{-1}. The pH was kept constant at pH 7; the duration of the preparation was 30 min. The resulting coacervate was washed several times with cold distilled water and stored at 4 °C; "Ca-polyP-Coa".Where indicated, the sequence of mixing was reversed: the polyP solution was added to the $CaCl_2$ solution.

The viscosity of the coacervate was determined using a Brookfield DV3T Rheometer (Brookfield, Middleboro; MA).

2.3. Preparation of Ca-polyP-NP

Amorphous nanoparticles of Ca-polyP, "Ca-polyP-NP", were prepared as described [23]. If not mentioned otherwise, a 2.5-fold molar excess of $CaCl_2 \cdot 2H_2O$ over the concentration of Na-polyP was used to prepare the NP. The solution was kept constant at a pH of 10 with NaOH. The reaction was continued for 12 h under stirring conditions. The obtained NP were washed in water and in ethanol and then dried (50 °C).

In one series of experiments, the polyP solution was poured into the $CaCl_2$.

2.4. Microscopic analysis

High resolution SEM (scanning electron microscopy) images were taken with a Zeiss Gemini 1530 (Zeiss Oberkochem; Germany). The samples were dried prior to mounting onto a microscope aluminum stub. The light microscopical images were taken with a VHX-600 Digital Microscope (Keyence, Neu-Isenburg, Germany). The TEM (transmission electron microscopy) analysis was performed with a Tecnai 12 microscope (FEI Electron Optics, Eindhoven; Netherlands) as described [24].

2.5. Fourier Transformed Infrared Spectroscopy

The material, dried NP or coacervate, was ground to a composite

powder and then analyzed by FTIR (Fourier Transformed Infrared Spectroscopy). The analyses were performed with an attenuated total reflectance-FTIR spectroscope/Varian IR spectrometer (Agilent, Santa Clara; CA).

2.6. Simulation method

The molecular mechanics and molecular dynamics simulations and predictions of interatomic forces between Ca^{2+} and polyP were performed using the Materials Studio-Discovery Studio packages and the Analysis Module in InsightII/Discover program (BIOVIA-Accelrys Inc., San Diego, CA, USA). The protocols are based on the data collected with the COMPASS force field algorithm [25,26]. After drawing the polyP chain with a length of 20 P_i units and subsequent implementation of the additional option "clean geometry" of the program, 16 polyP molecules together with 350 Ca^{2+} ions and an aqueous environment were computed, again in the "clean geometry" mode 1000-times until the data output reached a variation of <1%. Energy minimizing was performed in the presence of ~5000 water molecules at a density of 1.15 g cm^{-3}. The simulations were run at a temperature of 297 K.

2.7. PolyP release assay

The following samples were used. The respective polyP polymer either as free Na-polyP or in combination with particulate Ca-polyP-NP was embedded in a 2% aqueous hydrogel prepared from hydroxyethyl cellulose (HEC; Caelo, Hilden; Germany). After a heating step (121 °C under positive pressure), the HEC hydrogel was supplemented with 600 μg mL^{-1} of Na-polyP or 60 μg mL^{-1} of Ca-polyP-NP or the two components together (600 μg mL^{-1} of Na-polyP and 60 μg mL^{-1} of Ca-polyP-NP), as indicated under "Results". Samples (1 mL) were dispensed into 24-well plates and incubated with 2 mL Ham's medium/10% fetal bovine serum (FBS). Immediately after plating or after different time periods aliquots were taken and subjected to the enzymatic polyP determination procedure.

The release of polyP from the polyP-hydrogel was quantitated using the "Phosfinity" total polyphosphate quantification kit (Aminoverse B.V., 6361HK Nuth; Netherlands). This assay is based on the enzymatic degradation of polyP with a highly specific enzyme releasing orthophosphate, which is quantified using a colorimetric phosphate detection reaction. The absorbance is read at 882 nm in a spectrophotometric plate reader. First, the concentration of orthophosphate in the reaction mixture was determined at the beginning of the enzymatic reaction. The concentration values obtained were subtracted from the values in the assays at the end of the enzymatic reaction. The polyP material detected by the "Phosfinity" assay thus only quantifies polymeric polyP. A polymer-specific enzyme is used to quantitate the polyP. The amounts of polyP (with all chain lengths) were calculated based on a calibration curve using standard phosphates between 2 and 200 μM.

2.8. Preparation of the PVA matrices

A 4% PVA solution (poly[vinyl alcohol]; M_w 146,000–186,000; #363065 Sigma-Aldrich) was used to plate the A549 cells as described before [27]. The polymer was supplemented with 200 μg mL^{-1} of "Ca-polyP-NP" and 1 mL of the PVA hydrogel was pipetted into 24-well plates; "PVA/polyP:NP". After two washing cycles, the layer-covered wells were used to overlay A549 cells; 2 mL cell aliquots ($20 \cdot 10^3$ cells mL^{-1}). To process the polyP phase of the "Ca-polyP-NP" caged in PVA to the coacervate state, the "PVA/polyP:NP"-coated 24-well plates were incubated for 24 h with 2 mL of Ham's F-12K medium with 10% FBS. During this treatment, the nanoparticles in the wells were converted into the "PVA/polyP:Coa" coacervate layers.

2.9. Cultivation of A549 cells

To determine the ATP release, A549 cells (#86012804 Sigma, Taufkirchen, Germany), a human lung (carcinoma) cell line, were cultured in Ham's F-12K (Kaighn's) medium (#21127022; Gibco/Thermo Fisher Scientific, Dreieich; Germany) supplemented with 10% FBS, 1% penicillin-streptomycin, and 4 mM glutamine as described [28,29]. The cells were grown in 24-well plates in a humidified atmosphere of 5% CO_2 in air (37 °C).

Spreading experiments of A549 cells were performed in 24-well plates coated with 1 mL of the respective PVA matrix. The cells at a density of $20 \cdot 10^3$ cells mL^{-1} were suspended on the matrices in 100 μL. After incubation for 48 h, the cells were fixed (3.7% formaldehyde; 20 min), permeabilized, and subsequently immune-stained for the distribution of the cell surface associated mucin 1 with anti-mucin 1 (#PA5-81524; Thermo Fisher Scientific; dilution 1:1000) and then reacted with Alexa Fluor 488-conjugated goat anti-rabbit IgG secondary antibody (flashing in green) as described [29]. The nuclei were stained red with propidium iodide (#P4864; Sigma-Aldrich). The specimens were inspected with the fluorescence microscope (Olympus, Hamburg; Germany).

2.10. Uptake studies of the NP

The A549 cells at a density of $100 \cdot 10^3$ cells mL^{-1} were suspended on the "PVA/polyP:NP" layer and incubated for 3 h in medium/serum. Then the cells were removed from the substratum by gentle shaking and transferred to a non-supplemented PVA layer. After additional 3 h, the cells were fixed, embedded (LR-white resin [# 62661; Sigma-Aldrich]), sliced and contrasted [24], and then inspected by TEM.

2.11. Determination of the extracellular ATP level on polyP containing matrices

The ATP released to the extracellular space was quantified using the luciferin-luciferase-based Enlighten assay (Promega, Madison; WI, USA) as described [24]. The A549 cells were grown in 24-well plates until they reached 90–100% confluency. Then the cells were suspended in Ham's medium without serum and incubated for a further 2 h at a cell density of 10^6 cells mL^{-1}. The wells were coated with three different PVA matrices: PVA control, "PVA/polyP:NP", and "PVA/polyP:Coa". To stop the reaction, 0.5 mL aliquots were collected and transferred to chilled polypropylene tubes (#Z334006; Sigma) and centrifuged (12,000 g; 5 min; EBA 200; Hettich GmbH, Tuttlingen; Germany). Aliquots of 100 μL were taken from the supernatants and transferred to the luciferin–luciferase assay. The values obtained were correlated with a standard curve for ATP to obtain the level of ATP released from the cells. ATP concentrations are given as pmol 10^6 $cells^{-1}$. As additional controls, the cells were pre-incubated with 40 μM Ap_5A (P^1,P^5-di(adenosine-5′)pentaphosphate pentasodium salt; #D4022, Sigma), an inhibitor of ADK [30], or 1 mM LEV (levamisole hydrochloride; #L9756; Sigma), which inhibits ALP [31], for 10 min before cell seeding.

2.12. Staining of A549 cells for ALP

The cells were cultured on either a plain PVA surface or a polyP-supplemented PVA hydrogel (either "PVA/polyP:NP" or "PVA/polyP:Coa") at a cell density of $10 \cdot 10^3$ cells mL^{-1} and incubated in medium/serum for two days. When mentioned, the cultures were supplemented with 1 mM LEV. Then samples were taken, washed with phosphate-buffered saline containing 0.1% Tween-20 and fixed with 70% (v/v) ethanol. After a further washing cycle with PBS, the cells were reacted with the ALP staining solution (#ab242287, ALP staining kit; Abcam, Cambridge; UK) and washed again with PBS and inspected by light microscopy.

2.13. Statistical analysis

The analyses were carried out with the SigmaPlot 13.0 (Systat Software, Erkrath; Germany) and the resulting graphs were plotted with the help of GraphPad Prism 7.02 (GraphPad Software, San Diego; CA). At least five or ten (as indicated) replicates were performed for each series. The results are given as mean ± standard deviation. The paired *t*-test was applied to assess the significance of differences. The *p*-values < 0.01 are considered as statistically significant (*). When comparing members from different groups, these significant differences were also marked ($^{\&}$).

3. Results

3.1. Driving forces of "Ca-polyP-Coa" and "Ca-polyP-NP" formation

Both the polyP coacervate and the polyP NP form after the interaction between soluble anionic polyP (Na-polyP) and cationic Ca^{2+} ions ($CaCl_2$) in an aqueous environment. Broadly, the coacervate is formed at neutral pH, while NP form at pH ~10. During this process electrostatic attractions between the oppositely charged ions take place. However, since ion-dipole attraction forces must also be taken into account in ionic solutions, it is important to estimate not only the strength of the interionic bonds between the ionic compounds but also the strength of the ion-dipole forces [32]. To approach a solution, docking and molecular dynamics simulations were performed as described under "Materials and Methods". Using these algorithms, topographic interactions of the three partners (polyP [16 polyP molecules], Ca^{2+} [120 Ca^{2+} ions] and water [~5000 water molecules]) were predicted.

At pH 7, the three components form an almost random arrangement pattern right from the start. The Ca^{2+} ions are arranged in a mixing mode around the polyP molecules throughout the aggregate (Fig. 1 A and B). Likewise, the water molecules are evenly distributed in the assemblies. After masking the water, the random, stochastic organization of polyP and Ca^{2+} is evident (Fig. 1 B). After hiding the polyP, the arrangement of the water molecules in the center of the aggregates can be seen (Fig. 1 C).

The simulation pattern of polyP, Ca^{2+} and water at pH 10 shows a different pattern (Fig. 1 D–F). A clustering of the polyP molecules and partial separation of the Ca^{2+} ions is seen. It is obvious that under the settings input into the algorithm of the modeling system, the cationic Ca^{2+} becomes at least partially separated from the anionic polyP aggregations, indicating a shift between short- and long-range electrostatic interactions. Blinding out the polyP molecules highlights the presence of water within the polyP cluster (Fig. 1 F).

3.2. Kinetics of "Ca-polyP-Coa" and "Ca-polyP-NP" formation

Compared to the NP formation, the process of "Ca-polyP-Coa" formation (at pH 7) is a slow process. Starting with a solution of 0.48 M Na-polyP into which 1.2 M $CaCl_2$ is introduced, the first increase in turbidity is seen after ~9.5 mL of $CaCl_2$ (Fig. 2 I–A). Later in the course of aggregate formation (as mentioned later, coacervates are formed at pH 7), the turbidity decreases again and levels off at 20% after ~25 mL. The resulting aqueous aggregate has a viscosity of 10–15 cP. The kinetics of coacervate formation, measured by dynamic viscosity, is independent within the temperature range 14 °C and 55 °C.

Very much faster is the aggregate formation at pH 10, which reflects the formation of the nanoparticles "Ca-polyP-NP" (Fig. 2 I–B). Under these higher pH conditions, the turbidity increases almost immediately. The high turbidity remains constant during the subsequent preparation period.

By eye inspection, the difference in the kinetics of aggregate formation at pH 7 and pH 10 becomes obvious (Fig. 2 II-A and B). At pH 7, the first aggregate can be seen after addition of 6 mL of $CaCl_2$ and the fluffy, bulky coacervate deposits appear after ~10 mL (Fig. 2 II-A). Again in contrast to the formation at pH 7, the first solid flocs appear already after 0.5–1.5 mL of $CaCl_2$ (Fig. 2 II-B) and the turbid appearance forms after the addition of ~10 mL. Even after mixing is stopped the material does not sediment during a 30-min incubation period.

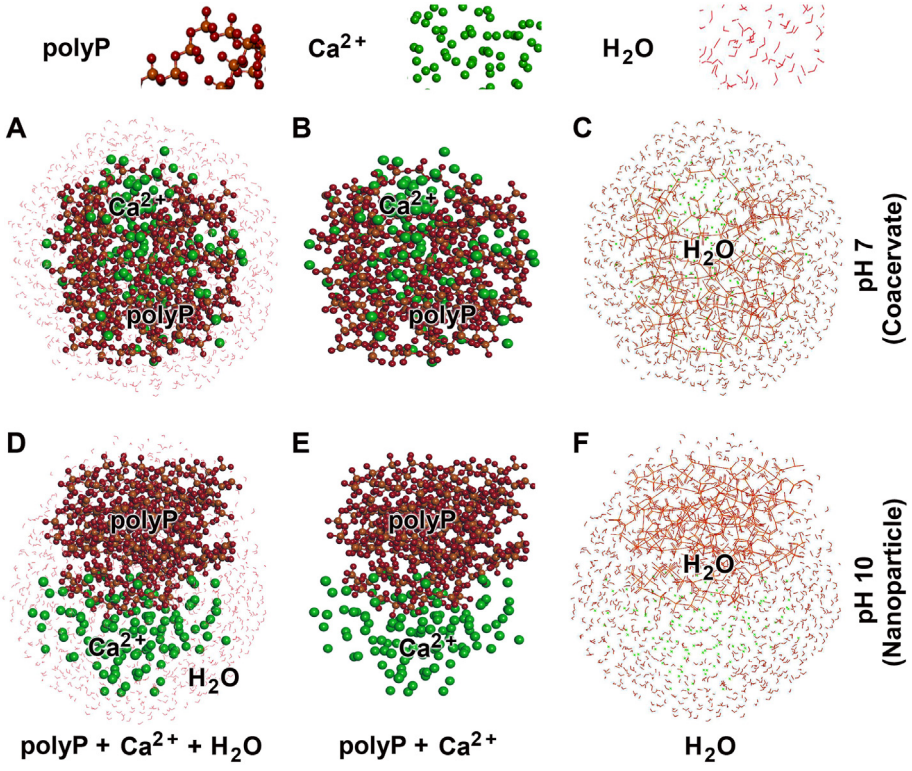

Fig. 1. PolyP (chain length of 20 P_i units) interacting with Ca^{2+} and water at (**A**–**C**) pH 7 and (**D**–**F**) pH 10. At neutral pH, the three components of the aggregates, polyP, Ca^{2+} and water, are arranged stochastically, while at pH 10 a clustering of the polyP molecules and a distinct separation of the Ca^{2+} ions are found.

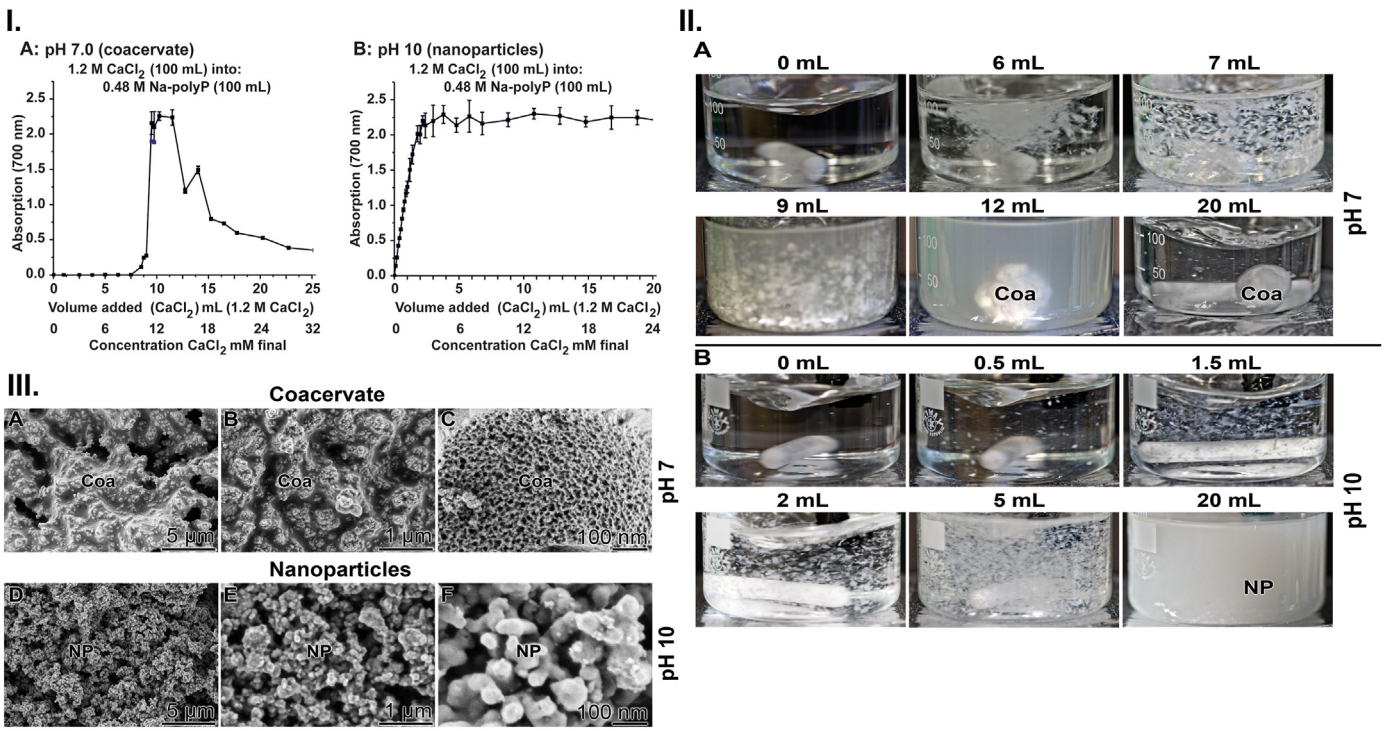

Fig. 2. Kinetics of pH-dependent aggregate formation. (**I.**) Turbidimetric titration analysis at pH 7 and pH 10. (**A**) At pH 7.0 (condition routinely used for coacervate formation) and (**B**) at pH 10 (usually selected for nanoparticle formation), solutions of 1.2 M $CaCl_2$ were poured into 0.48 M Na-polyP in a volume-controlled manner. The change of the turbidity was followed by measuring the changes in the absorbance at 700 nm. (**II.**) Optically visible aggregate formation from $CaCl_2$ and Na-polyP. Volume-controlled appearance of aggregates either at (**A**) pH 7.0 or (**B**) pH 10. It is apparent that the first aggregates appear later at pH 7 (after 6 mL) compared to the assay run at pH 10 (0.5–1.5 mL). According to SEM inspection, the aggregates at pH 7 are coacervates (Coa), while at pH 10 nanoparticles (NP) are formed. (**III.**) SEM analysis of the aggregates formed at (**A** to **C**) pH 7, coacervates (Coa), or (**D** to **F**) pH 10, nanoparticles (NP).

3.3. pH-dependent morphology and FTIR spectral analysis of coacervate and NP depositions

Morphology: Following the initial procedure [23], adding $CaCl_2$ (in a 2.5-fold molar excess) to the polyP solution, the dense aqueous coacervate forms at a pH of 7 (Fig. 2 III-A to C). The appearance of the dense/aqueous electrostatic complex after drying the sample on the stub is a continuous, slightly granular layer. The diameter of the granules is ~200 nm (Fig. 2 III-B). They are porous with holes of ~10 nm (Fig. 2 III-C).

If – under the same concentration conditions – the reaction is run at pH 10, only nanoparticles with a size range of 80–120 nm appear (Fig. 2 III-D to F).

FTIR: Differential infrared spectroscopy was performed on the material obtained by pouring the $CaCl_2$ solution into the polyP solution. The spectrum of the material at pH 7 (coacervate) differs from that collected at pH 10 (NP). The characteristic signatures for polyP are the signals at the following wavenumbers (Fig. 3 I-A and B), which are in the 1350−700 cm^{-1} range: 1255 cm^{-1} for $\nu_{as}(PO_2)^-$ [the bridging phosphate] versus $\nu_{as}(PO_3)^{2-}$ [the terminal phosphate units]; the absorption bands of ν_{as}(P–O–P) as the asymmetric stretching modes of the P–O–P linkages within polyP and the symmetric stretching ν_s(P–O–P), which also reflects the P–O–P linkages, are around near 900 and 750 cm^{-1}, respectively [33–35]. The signal at 1255 cm^{-1} for $\nu_{as}(PO_2)^-$ is known to shift to lower frequencies when divalent cations replace Na at this negatively charged site [O═P–O^-] [36]. Within a limited range, the wavenumbers given here shift from those of Na-polyP.

Looking at the aggregates that form from Na-polyP after addition of $CaCl_2$, at pH 7, the characteristic features were not only detected for Na-polyP, but also for "Ca-polyP-Coa" [12]. It should be stressed that at pH 7 the $\nu_{as}(PO_2)^-$ signal can be seen both in the spectrum for Na-polyP and for the coacervate "Ca-polyP-Coa" (Fig. 3 I–B). The corresponding SEM image is shown in Fig. 3 II-A. In contrast, at pH 10, the pH condition at which the nanoparticles "Ca-polyP-NP" are formed (Fig. 3 II-C), this $\nu_{as}(PO_2)^-$ signal almost completely disappears and remains as a shoulder of the strong $\nu_{as}(PO_3)^{2-}$ signal (Fig. 3 I–B). This change is most likely due to the binding of Ca^{2+} to the internal phosphate units.

Indicative is the change of the $\nu_{as}(PO_3)^{2-}$ signal if the $CaCl_2$ solution is not dropped into the polyP solution, but Na-polyP is added to the $CaCl_2$ solution in the reverse order (Fig. 3 I–C). Under this condition, the $\nu_{as}(PO_2)^-$ signal is seen around ~1250 cm^{-1} not only at pH 7 but also at a pH 10. From this finding it was deduced that the $\nu_{as}(PO_2)^-$ units undergo immediate binding to the fully available Ca^{2+} ions.

Morphology - sequence dependence ($CaCl_2$ – Na-polyP): The morphology of the Ca^{2+}: polyP salts is dependent on the sequence in which the two starting solutions are mixed together. This fact becomes visible by SEM analysis. According to the initially described sequence of adding $CaCl_2$ solution to Na-polyP solution [23], the coacervate is formed at pH 7, while nanoparticles develop at pH 10 (Fig. 3 II-A *versus* –C). If Na-polyP is added to the $CaCl_2$ solution at pH 7, Ca^{2+}/phosphate deposits are formed, which are identified as coacervates by SEM (Fig. 3 II-B). Surprisingly, bulky coacervate depositions are also formed at pH 10, as identified by SEM (Fig. 3 II-D) and confirmed by FTIR (Fig. 3 I–C). Hence, under these pH 10 conditions and when 100 mL of a 0.48 M Na-polyP solution is added to 100 mL of a 1.2 M $CaCl_2$ solution, coacervate deposits are formed over the complete reaction process. The additional SEM image in Fig. 3 II-E (pipetting scheme: 100 mL of 1.2 M $CaCl_2$ added to 100 mL of a 0.48 M Na-polyP solution) shows the pronounced porous morphology in the developed NP.

The coacervate-like polyP phase is probably caused by a strong and rapid binding of the Ca^{2+} ions to the polyP polyanions as soon as the Na-polyP solution is added to the $CaCl_2$ solution. In turn, no sorting out of Ca^{2+} from polyP ions takes place, which has been predicted for the interaction of the two ions during the addition of $CaCl_2$ to Na-polyP (Fig. 1 E). This assumption is also consistent with the published data [37].

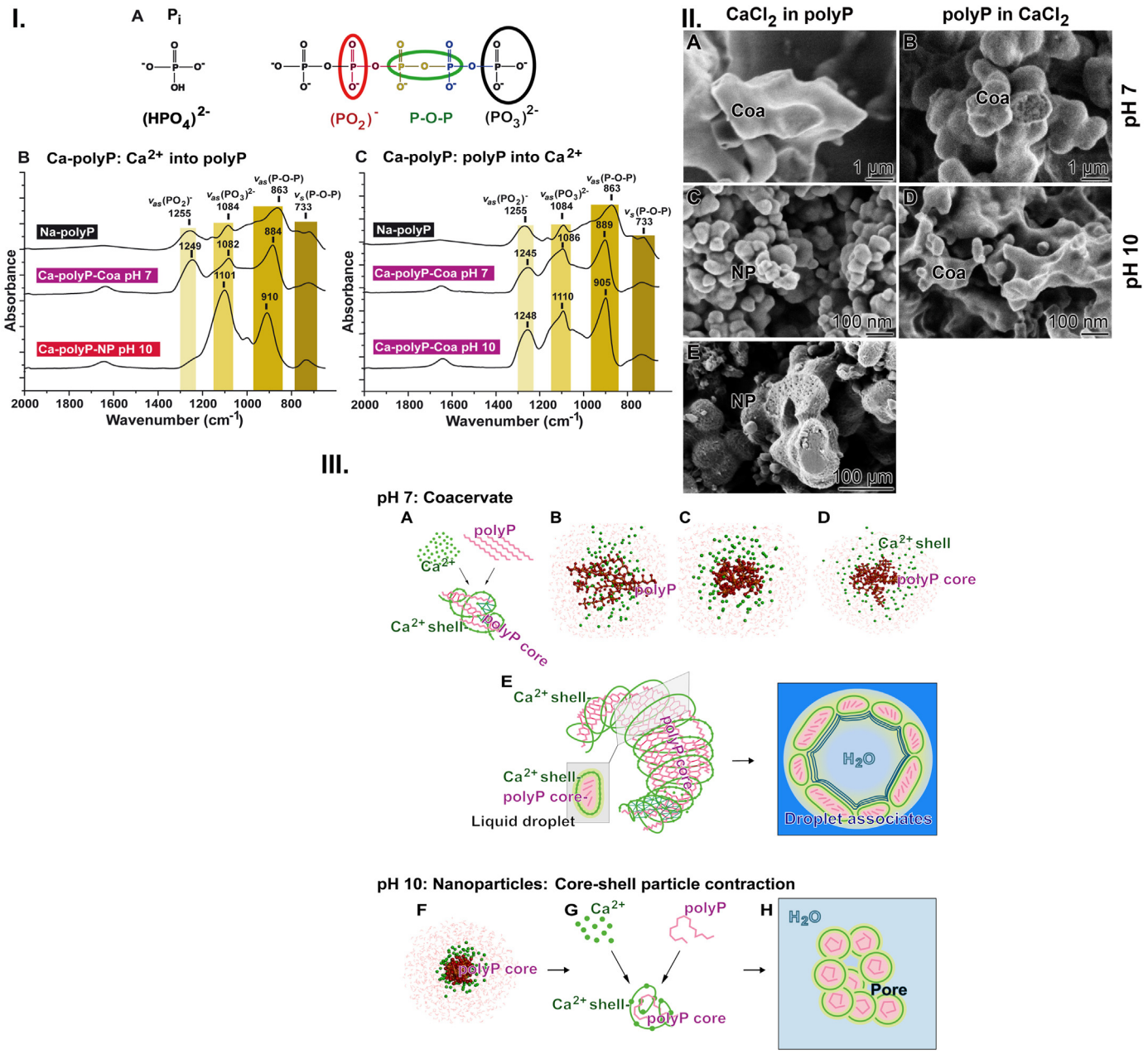

Fig. 3. Characterization of the Ca^{2+} - polyP aggregates. (**I.**) FTIR analyses of the aggregates. (**A**) The characteristic sites within polyP are highlighted in the infrared spectra. (B) Comparison of the FTIR spectra of the aggregates formed after addition of $CaCl_2$ in Na-polyP solution. The reactions were performed at pH 7 or pH 10. It is striking that the signature for $(PO_2)^-$ is only visible in the product at pH 7 (coacervate), but not in the sample at pH 10 (nanoparticles). (C) In the reverse sequence, addition of Na-polyP solution into $CaCl_2$ solution, the characteristic peak for $(PO_2)^-$ remains both at pH 7 and pH 10. (**II.**) SEM analysis of the particles, nanoparticles (NP), or the coacervate liquid phase aggregates (Coa) formed in the pipetting scheme (A and C) $CaCl_2$ into Na-polyP or (B and D) polyP into $CaCl_2$ in both the pH 7 and the pH 10 environment. (E) Porous internal morphology of NP formed in the $CaCl_2$ into Na-polyP pipetting sequence. (**III.**) Snapshots taken during the molecular dynamics simulations at (**A** to **E**) pH 7 (coacervate) and (**F** to **H**) pH 10 (nanoparticles). At pH 7, the two components (A) $CaCl_2$ and Na-polyP (B) initially arrange themselves randomly (optimization steps: 5) and subsequently sort each other out (C, steps: 50; and D, steps: 75) and form a polyP core and a Ca^{2+} rich shell. (E) The respective Ca^{2+} shells form a ribbon around the polyP core and give rise to small liquid droplets that fuse together and trap water within the droplet associates. (F) At pH 10, the two components evolve into contracted core-shell particles (optimization steps: 70), which associate (G and H) to nanoparticles comprising only small internal pores.

Interatomic forces predictions: The calculation of the interacting forces of Ca^{2+} and polyP revealed a re-location movement of the two partners as a function of time (Fig. 3 III). At pH 7, the two components Ca^{2+} and polyP (Fig. 3 III-A) organize themselves rather randomly, while in the following steps the two interacting members sort apart and finally form two concentric rings with the Ca^{2+} on the outside and polyP as the core (Fig. 3 III-B to D). It can be predicted that these assemblies form the liquid droplets (Fig. 3 III-E) with the polyP inside (core) and the Ca^{2+} ions around it [38]. The ions are surrounded with hydrate shells [39,40], allowing the droplets to merge and form the water-rich coacervate. At pH 10, the components Ca^{2+} and Na-polyP also form a concentric ring pattern, but this is more dense (Fig. 3 III-F). This dynamic is based on the stronger affinity of Ca^{2+} for the more ionized polyP, especially since at pH 10 the second OH of the phosphate end-groups of the polymer ($pK_{a\text{-}2}$ of 7.09) is also almost completely dissociated. Consequently, the liquid droplets formed at pH 7 are larger than the particles at pH 10 (Fig. 3 III-E

versus Fig. 3 III-F to H). As the "Ca-polyP-NP" nanoparticles are dried, the water in the pores is removed.

3.4. Differential polyP release kinetics from nanoparticles versus coacervate

The release of polyP was determined from a HEC hydrogel embedded either with Na-polyP alone (600 μg mL^{-1}) or in combination with "Ca-polyP-NP" (60 μg mL^{-1}). These concentrations and concentration ratios were chosen because the optimal effect on wound healing could previously be achieved with them. When the release of polyP from the hydrogel was determined with Na-polyP alone (600 μg mL^{-1}), ~40% of the polymer was released during the first 2 d; an additional ~20% was released at day 4 (Fig. 4 I–A). After 9 d, 72% (434 μg mL^{-1}) of the Na-polyP polymer was found in the medium/serum surrounding the sample. The kinetics show that most of the polymer is set free during the first 4 days. The comparison of the determined released polyP from the hydrogel supplemented with Na-polyP (600 μg mL^{-1}) alone with that together with "Ca-polyP-NP" (60 μg mL^{-1}) showed values that do not differ significantly (Fig. 4 I–A). In principle, this result was to be expected, since Na-polyP was present in the hydrogel in a 10-fold excess over "Ca-polyP-NP".

Therefore, the release kinetics from the hydrogel was determined with "Ca-polyP-NP" as the sole component. In this series of experiments, a clear difference in the kinetics was evident compared to the results obtained with the gel containing both Na-polyP and nanoparticles (Fig. 4 I–B). During the first 4 d of incubation, only a non-significant increase in polyP was measured in the assays with "Ca-polyP-NP" alone. The increase becomes significant after an incubation period of 6 d with ~37%. Extending the incubation period to 9 d resulted in a release of 69% (41 μg mL^{-1}) of the polymer from the particulate "Ca-polyP-NP". From the data in Fig. 4 I, it is concluded that the release of polyP from the gel containing the Na-polyP is almost twice as fast compared to the hydrogel supplemented with particulate polyP.

3.5. Transformation of nanoparticles into the coacervate phase

In an earlier report, we showed that the high zeta potential of the nanoparticles is reduced in the presence of peptides, leading to the transformation of the nanoparticles into the coacervate phase [12]. This process is now supported by FTIR and also SEM analyses.

As shown above (Fig. 3 I–B), the $\nu_{as}(PO_2)^-$ signal in the FTIR spectrum of the Ca-polyP coacervate, which is present as a distinct peak at a wavenumber of 1255 cm^{-1}, changes into a flat shoulder in "Ca-polyP-NP". This signal is also not present in the polyP-free PVA matrix (Fig. 4 II); again, this $\nu_{as}(PO_2)^-$ band, which is ascribed to the stretching vibrations of $(PO_2)^-$, is absent in the PVA layer with "Ca-polyP-NP", the "PVA/polyP:NP" hydrogel. However, when this layer is incubated for 24 h with Ham's medium/FBS, the $\nu_{as}(PO_2)^-$ signal at 1256 cm^{-1} can be clearly seen, indicating that the nanoparticles in the PVA hydrogel undergo a conversion to the coacervate phase, "PVA/polyP:Coa" (Fig. 4 II).

This conversion is also seen in microscopic images (Fig. 4 III). The surfaces of the PVA hydrogel are flat (Fig. 4 III-A) in contrast to the matrix supplemented with "Ca-polyP-NP" (Fig. 4 III-B). After incubation with medium/serum, polyP undergoes a transformation into a flat coacervate gel (Fig. 4 III-C and D).

3.6. Increased spreading of A549 cells on polyP-enriched PVA matrices

The A549 cells were plated in 24-well plates coated either with the nanoparticles "PVA/polyP:NP" or with the coacervate obtained from the NP phase by incubation with medium/serum "PVA/polyP:Coa" (Fig. 5 I). The cells attached to the particulate polyP phase have a large size (~50 μm) and show a scattered distribution pattern and the nuclei are flat (Fig. 5 I-A and C). The cytoplasm was stained with mucin 1 antibodies and the nuclei with propidium iodide. The increase in the growth number during the 24 h incubation period was determined to be 47.1 ± 7.3%. In contrast, the cells grown on the coacervate phase of polyP are densely packed and their nuclei are arranged in condensed, massy cell bodies

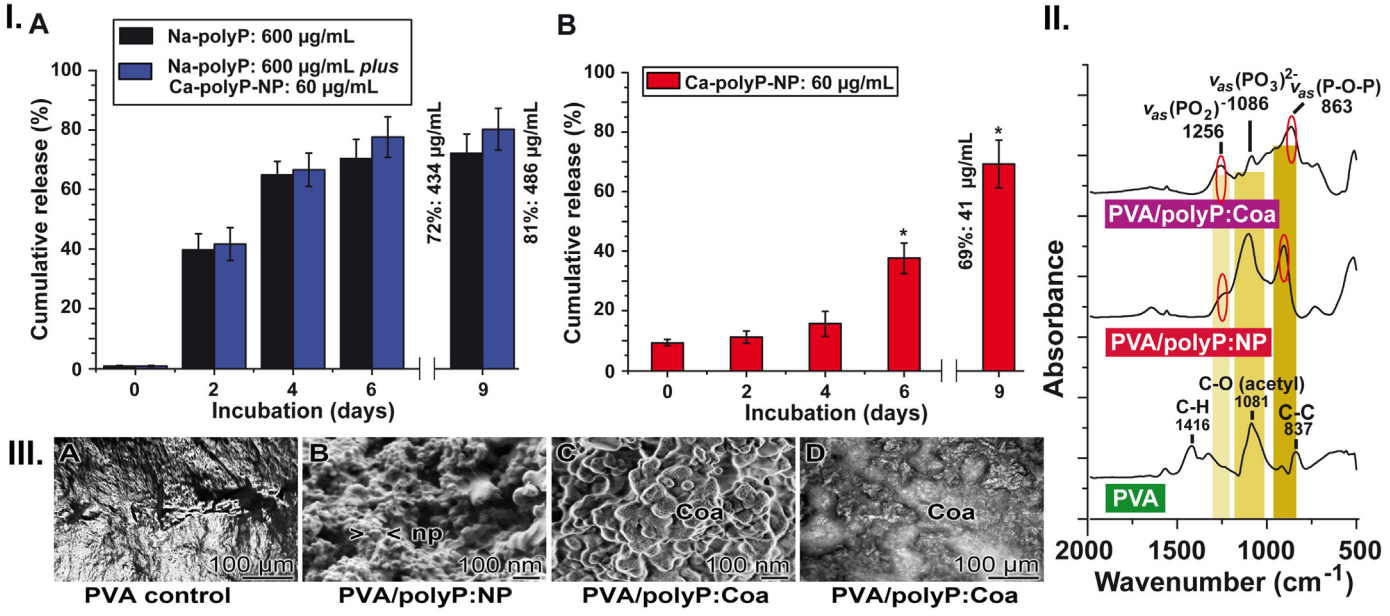

Fig. 4. Release of polyP and transformation of the particulate "Ca-polyP-NP" into the coacervate phase. (**I.**) PolyP release from HEC hydrogel. (**A**) Na-polyP (600 μg mL^{-1}) or Na-polyP (600 μg mL^{-1}) together with "Ca-polyP-NP" (60 μg mL^{-1}) were embedded into the hydrogel. The released polyP was determined in the Phosfinity assay. (**B**) In a separate series, the release of polyP from the hydrogel with "Ca-polyP-NP" (60 μg mL^{-1}) was determined. Ten separate determinations were performed; the means ± SD are given. (**II.**) FTIR analyses of plain PVA gel as well as of "PVA/polyP:NP" hydrogel and "PVA/polyP:Coa" hydrogel formed after incubation with medium/serum. In the coacervate hydrogel, the characteristic $\nu_{as}(PO_2)^-$ signal is present (circled). Also visible is the ν_{as}(P–O–P) peak reflecting the polyP polymer. (**III.**) Microscopic images reflecting the phase transformation of the nanoparticles (np) into the coacervate (Coa) phase. (**A**) Surface of the plain PVA hydrogel; optical microscopy. (**B**) PVA supplemented with "Ca-polyP-NP" with 100 nm nanoparticles (np); SEM. (C) Surfaces of the coacervate phase (Coa), PVA/polyP:Coa, at high (SEM) and (D) low magnification (optical microscopy).

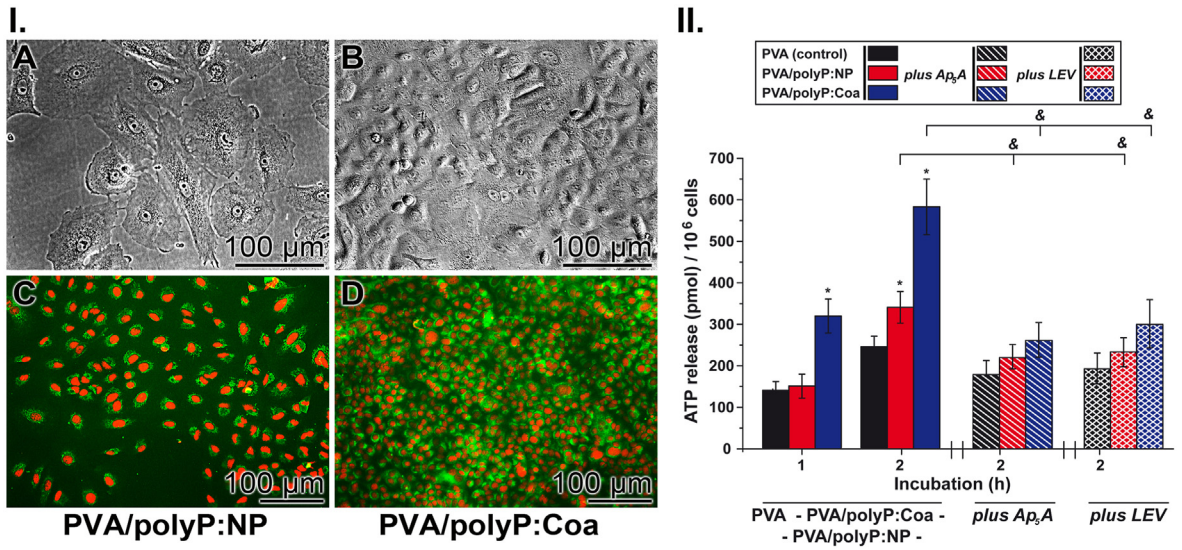

Fig. 5. Increased biological activity of A549 cells after cultivation on PVA polyP coacervate, "PVA/polyP:Coa". (**I.**) Different cell morphology of A549 cells cultured for 48 h on (**A** and **C**) particulate "Ca-polyP-NP" ("PVA/polyP:NP") versus those contacted with (B and D) "PVA/polyP:Coa". On the coacervate layer, the density of the cells is higher and the cell bodies are more compact compared to the particulate polyP in PVA. (**II.**) Response of A549 cells to different polyP environments. The cells were suspended on PVA layers, either on PVA control (black bars), particulate "PVA/polyP:NP" (red bars) or on "PVA/polyP:Coa" (blue bars) and incubated for 1 h or 2 h. Then the supernatants were collected and the ATP content determined using the luciferin-luciferase-based Enlighten assay. Significant pairs are marked (*$p < 0.01$). In parallel series, the effect of the ADK inhibitor Ap_5A (hatched) and the ALP inhibitor LEV (cross-hatched) on the ATP production of A549 cells cultured onto the three different matrices was determined as well. Significant differences are marked ($^{\&}$ $p < 0.01$).

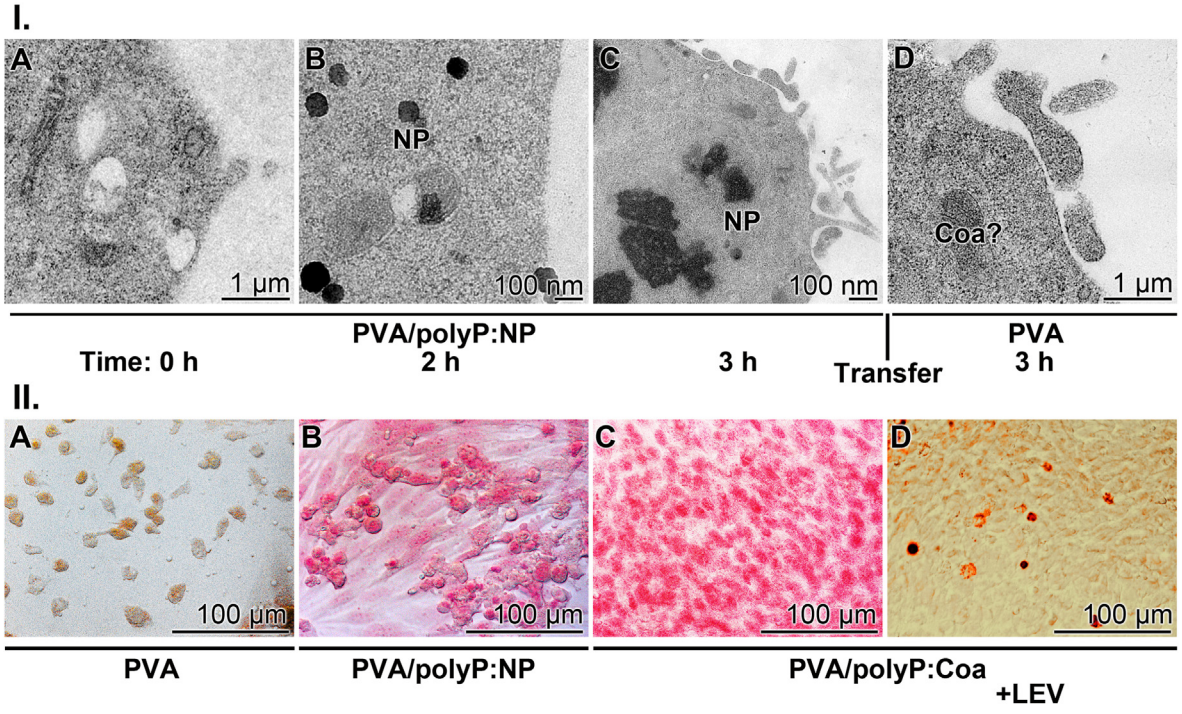

Fig. 6. NP in the cytoplasm of A549 cells and distribution of ALP in A549 cells, the enzyme that hydrolyzes the polyP in NP. (**I.**) Uptake kinetics of polyP NP by A549 cells; TEM. (**A**) At time zero, no nanoparticles (NP) can be seen. (**B** and **C**) After incubation onto the "PVA/polyP:NP" layer for 2 h or 3 h, (**D**) the cells were transferred on a non-supplemented PVA substratum and incubated for a further 3 h. On the "PVA/polyP:Coa" layer, the cells take up NP. The NP are absent on the plain PVA surface; the darker shaded areas could represent coacervate areas (Coa?). (**II.**) Increased expression of ALP in A549 cells cultured on "PVA/polyP:Coa"; light microscopy. (**A**) The cells growing on the hydrogel without polyP ("PVA") for 2 d show a low staining reaction and only a scattered distribution pattern compared to those cultured on (**B**) "PVA/polyP:NP". (**C**) In cultures on "PVA/polyP:Coa", however, the staining is significantly stronger and the density of the cells is higher. (**D**) Suppression of the staining reaction after addition of the ALP inhibitor LEV to cultures on "PVA/polyP:Coa".

(Fig. 5 I–B and D). During the 24 h incubation, the cell number increased by 73.0 ± 5.6%.

3.7. ATP release from A549 cells on coacervate versus nanoparticles

The A549 cells react differently when cultivated on either the PVA-control matrix, the PVA-based matrix supplemented with "Ca-polyP-NP" (200 μg mL^{-1}), "PVA/polyP:NP", or on the coacervate phase of polyP. The A549 cells grown on the "PVA/polyP:NP" responded after a 2-h incubation period with a small but significant release of ATP compared to PVA without polyP. In contrast, the cells attached to "PVA/polyP:Coa" layers produce a strong ATP burst already after 1 h, which is significant and ~150% higher compared to the PVA control and the "PVA/polyP:NP"-supplemented layer (Fig. 5 II). After a further 1 h, the ATP release on the coacervate layer increases by about two-fold.

The ATP production by the A549 cells is significantly inhibited by the ADK inhibitor Ap_5A and also by the ALP inhibitor LEV with all different PVA matrices (Fig. 5 II).

3.8. Uptake of NP into A549 cells

The cells were first incubated in medium/serum on a "PVA/polyP:NP" layer. Samples were taken at time 0 and after incubation for 2 and 3 h. Then the cells were removed from the polyP-supplemented matrix and transferred to a non-supplemented PVA layer and the incubation was continued for 3 h. Slices from embedded cells were inspected by TEM (Fig. 6 I). At time 0, no NP are visible in the cut cells (Fig. 6 I–A). After a 2–3 h, NP accumulate in the cytoplasm (Fig. 6 I–B and C). Then the cells were transferred to a polyP-free PVA layer and incubated for a further 3 h (Fig. 6 I–D). After this period, no distinct, electron-dense particles can be seen in the cytoplasm; only clusters of diffuse darker shaded areas are visible, presumably reminiscences of coacervate droplets.

3.9. Effect of polyP on the expression of ALP

To assess the effect of the different polyP phases on ALP expression, A549 cells were seeded on following surfaces: plain PVA, "PVA/polyP:NP" or "PVA/polyP:Coa". After an incubation period of 2 d, the cells were subjected to a specific ALP staining. In the case of the PVA cultures, only a very low cell density is visible on the PVA matrix (Fig. 6 II-A). The degree of staining of cells cultivated on "PVA/polyP:NP" is higher (Fig. 6 II-B). However, an incomparably high staining level is seen for those cells grown on "PVA/polyP:Coa" (Fig. 6 II-C); when these cultures with "PVA/polyP:Coa" were additionally exposed to 1 mM LEV, the red/purple staining of the cells is almost completely reduced (Fig. 6 II-D).

4. Discussion

First of all, inorganic NP made from native or processed metals are stable in a biological environment, possibly also inert, such as gold, silver, copper, and aluminum NP. This property stems from their inherent antibacterial activity and/or in vitro cytotoxicity. They obtain their bio-medical impact due to their antibacterial function [41]. Among the inorganic nonmetallic materials constituting NP, those based on phosphate or silica gained bio-medical impact [42–45] because they are soluble (can form a dispersion) under physiological conditions. A new area started when it was possible to prepare polyP-NP that elicit regenerative activity [46] in a bioinspired way [23]. The special feature of these polyP-NP is that they undergo a transition from an "inert" and consistently stable NP state into a physiologically active coacervate phase [12]. In the extracellular space, both unprocessed polyP and Ca-polyP-NP are transported via the blood platelets through the blood vessels [6,7,47]; Fig. 7. Both short-chain polyP (~50 P_i units) and longer-chain polyP (~150 P_i units) are transported via these cell fragments and released from them upon activation. In the circulating blood, the polyP

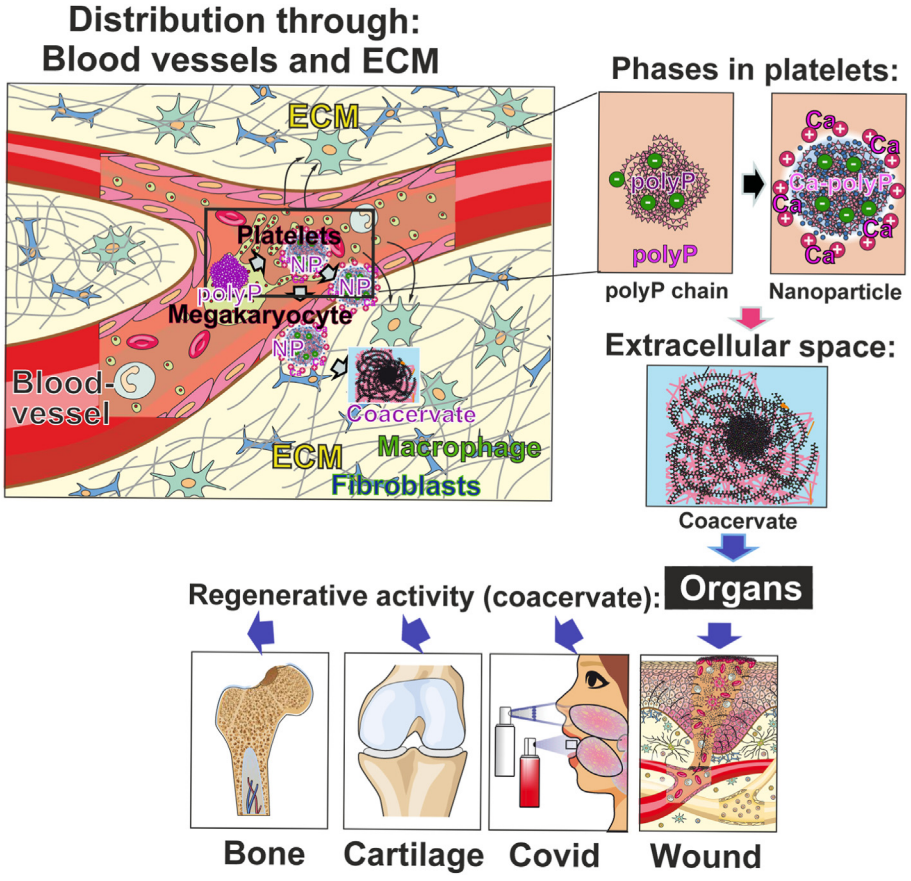

Fig. 7. Site of polyP formation and its distribution pattern in humans. **Left panel:** Every cell contains polyP with the highest concentration in the large bone marrow cells, the megakaryocytes (size between 50 and 150 μm). From these precursor cells 2–3 μm small platelets are formed and released into the bloodstream; one megakaryocyte produce 1000 to 3000 platelets. In these blood cells the chain-shaped polyP undergo with Ca^{2+} the transition to Ca-polyP-NP of a 100 nm size. **Right panels:** The phases of polyP processing: polyP chain to nanoparticle, and finally and in particular in the extracellular matrix system (ECM) to coacervate. Bottom: Always, when a damaged organ is under regeneration, blood platelets deliver the polyP components, like in bone, cartilage, viral tissue damage (e.g. Covid) or wounds, which contribute to the restoration.

incorporated into NP remains attached to the platelet surface while the soluble polymer chains are set free. When the platelets are exposed to ECM, they are activated by interaction with collagen and laminin, and also with fibrinogen in vascular events [48]. The activation of the platelets upon contact with ECM proteins occurs via their adhesion receptors, especially when the endothelial barrier is disrupted [49]. PolyP in the circulating blood or plasma has a half-life of ~1.5–2 h [50], compared to platelets, which persist for 7–10 d and constitute a density of 150–400 · 10^3 platelets per mL. In addition to the platelets, macrophages contain large amounts of polyP [51]. These migration competent cells, which are important for the inflammatory status, produce migrasomes, which are loaded onto retraction fibers that trail behind these migrating cells, the podocytes [52]. The migrasomes are vesicular structures filled with cellular contents and small vesicles. Platelets also produce migrasomes, which they release after activation [53]. It is to be expected that Ca-polyP-NP are also involved in this recently published cell migration pathway.

PolyP is an essential buffering molecule in eukaryotic cells [54]. More specifically, it has been reported that polyP is a crucial molecule especially in the mitochondria, where this polymer controls the Ca^{2+} exchange across the mitochondrial inner membrane and calcium-buffering system within the matrix [55].

PolyP-NP undergo coacervation in the presence of peptides especially in the extracellular space. This process is supported by the aqueous environment of the ECM which is also rich in Ca^{2+} [12]; Fig. 7. Through the blood vessels and the ECM, polyP is distributed to the different organs, bone, cartilage and to wounds and, if present, also to viruses such as coronavirus 2 [56,57]; Fig. 7. In the liquid gel-like phases (intra- and extracellular sites), polyP undergoes enzymatic hydrolysis in the presence of ALP, a process that, together with ADK, initiates ATP generation [21]. Both enzymes occur in the intra- and extracellular space as well as cell surface-associated [12,58]. Furthermore, Ca-polyP-NP are taken up intracellularly via an endocytosis mechanism [59]. There, the NP remain closely associated with the cell and form sites where intracellular coacervation also takes place [60].

The aim of the present study was to elucidate and model the initial events of the coacervation process of polyP, its pH dependence and – importantly – its phase-dependent effect on the physiological generation of extracellular ATP [21]. Again, as defined, coacervates are formed as condensed liquid-like droplets between oppositely charged polymers. However, the polyP coacervates form in the presence of polyP together with divalent, "monomeric" cations. A series of coacervation studies of Na-polyP with divalent (e.g., Ca^{2+} and Mg^{2+}) but also trivalent (e.g. Al^{3+}) cations have been performed and published [61,62], mainly focusing on material science. Here we focus on a biomimetically engineered NP fabrication process that is also used in nature to deposit polyP in cell organelles, specifically in the acidocalcisomes [16].

High concentrations of polyP with a chain length between 40 and 150 P_i units are present in the acidocalcisomes (reviewed in: [21]). In the protozoan *Trypanosoma cruzi*, these organelles contain not only polyP (~1400 mmol kg^{-1}) but also high levels of Mg^{2+} (650), Ca^{2+} (170), Zn^{2+} (150), and Na^{+} (160) [63]. Consequently, the polymer is present in these organelles as free chains (Na-polyP) or particulate Ca-polyP-NP. The fabricated Ca-polyP-NP [23] or Mg-polyP-NP [64] have a size of around 100 nm, are porous [46], and have a high zeta potential with the consequence that the particles have a high stability [12]. Despite this physical property that causes repulsive electrostatic forces of the particles resisting aggregation, the Ca-polyP-NP are distinctly biocompatible and evoke a pronounced regenerative activity in vivo [65]. When applied to bone defects, the particles are resorbed and induce new hydroxyapatite mineral deposition at this site. The unprecedented feature of these polyP-NP is their characteristic phase transition from the NP state into an aqueous coacervate in the physiological environment. This process is driven by peptides in the body fluids that lower the zeta potential and cause the transition into the coacervate state [12]. In this conversion, the size of the polyP chains (~35 P_i units) and the Ca:P atomic ratio 1.78 remain unchanged (starting from a NP preparation at a $CaCl_2$ to Na-polyP weight ratio >2.5) [23].

So far, there are no data that indicate differences between the physiologically occurring polyP fractions, the medium-chain polyP molecules (around 40 P_i units) compared to the longer-chain polyP molecules (≈400 P_i units). Since the water solubility of both polymer fractions is not dramatically different at room temperature, there is presently no reason to assume that these polyP fractions differ to a greater extent in their tendency to form coacervates.

Under conventional conditions, adding the $CaCl_2$ solution to the polyP solution, the coacervate is obtained at pH of 7 while the NP are formed at pH 10. Applying the simulation approach using molecular mechanics and molecular dynamics algorithms, a drastic difference in the distribution patterns of the polyP chains and the Ca^{2+} ions at pH 7 and pH 10 is found. At pH 7, the condition under which the coacervate is formed, there is a random distribution of the polymers and Ca^{2+} (Fig. 1), allowing liquid droplets to develop along the Ca^{2+} shell surrounding the polyP core (Fig. 3 III). In contrast, at pH 10, the condition favoring NP formation, a compartmentalization of Ca^{2+} from polyP occurs, followed by compression of the initial core-shell particles. In contrast to NP formation, coacervate is a time-delayed process. The FTIR absorption spectra show a distinct difference between the Ca-polyP coacervate and NP by the presence of the antisymmetric stretching vibration of the bridging for the $(PO_2)^-$ in the coacervate [33]. At present, we attribute the disappearance of the $\nu_{as}(PO_2)^-$ signal in the Ca-polyP-NP to interaction with the binding Ca^{2+} ion. Surprisingly, when the polyP solution is added to the $CaCl_2$ solution, the $(PO_2)^-$ signal remains in the formed deposits both at pH 7 and at pH 10, indicating that a coacervate is formed under both conditions. The SEM analyses confirmed this implication and suggest immediate binding of the Ca^{2+} ions, initially present in large excess, to the polyP polyanions during the addition of the polymer, preventing the contraction of the core-shell liquid droplets. Therefore, under the pH 10 conditions and when 100 mL of the 0.48 M Na-polyP solution is slowly added to 100 mL of the 1.2 M $CaCl_2$ solution, coacervate deposits are formed over the complete reaction process. The formation of this phase of the Ca-polyP salt can best be explained by the assumption that already at the beginning of the Na-polyP addition to the $CaCl_2$ solution, in the presence of the initially large excess of Ca^{2+} ions, there is a strong and immediate binding of Ca^{2+} ions to the polyP polyanions, which is certainly strong at pH 10. In turn, no sorting of Ca^{2+} from the polyP ions is favored, which was predicted for the interaction of the two ions during the addition of Ca^{2+} to polyP (Fig. 1 E). This assumption is also consistent with the published data showing that the occupation of the Ca^{2+} binding sites and the strength of binding on the polyP chain during the coacervation process is critically dependent on the Ca^{2+}/polyP ratio [37,66].

The release kinetics of polyP from the Ca-polyP-NP determines the biological potency of the NP. The supplementation of the PVA hydrogel with Na-polyP already shows a strong increase in medium/serum after 2 d, which even increases in the four following days and has reached 72% after 9 d. The release kinetics of particulate Ca-polyP-NP has a lag phase of about 4 d and increases after 6 d and finally to 69% after 9 d. During this lag phase, the transformation from the NP to the coacervate phase proceeds, as determined by FTIR and microscopic analysis.

The remarkable biochemical feature of polyP is the presence of the high-energy phosphoanhydride bonds that link the P_i units within the polymer chain [67–69]. During enzymatic hydrolysis by ALP, starting from the termini of the polyP chain, the released free energy is partially stored in ADP, which is used for driving metabolic pathways (reviewed in: [21]). Subsequently, the phosphotransferase ADK catalyzes the interconversion of ADP to ATP and AMP. The generation of ATP from polyP is a fast process and takes place within 1–2 h [70]. In the present study, A549 cells were plated on a PVA hydrogel supplemented without or with polyP. After an incubation period of 48 h, the cells seeded on PVA with particulate Ca-polyP-NP show a lower cell density compared to cells on the polyP coacervate "Ca-polyP-Coa". Using this setting, the ATP generation and release from the cells on PVA without polyP was

significantly lower compared to the cells growing on particulate or even more on coacervated polyP. The key roles of the two enzymes ALP and ADK have previously been proven by inhibition studies with their inhibitors LEV and Ap_5A [71]. These results underscore the importance of the coacervate phase in achieving the optimal energy utilization of polyP. Furthermore, after exposure to the polyP coacervate, A549 cells express a higher level of ALP, a finding that is strengthened by a higher growth rate of the cells.

The cells growing on the PVA hydrogel were also used to gain insight in the fate of the polyP-NP after endocytotic uptake, which is inhibitable by trifluoperazine [59]. For this series, the cells were grown on the "PVA/polyP:NP" layer. After 2–3 h, the NP can be clearly seen in the cytoplasm by TEM visualization. This duration for particle uptake by endocytosis is within the range published for other systems [72]. After transfer to a polyP-lacking matrix, the NP disappear in the cytoplasm, leaving – apparently – space for coacervate droplets.

By definition, as mentioned, a coacervate, especially a coacervate of the complex type, is built from colloidal droplets formed by liquid–liquid phase separation in a solution containing both polycations and polyanions [73]. In contrast, proteinaceous gelatin-alginate coacervates are formed according to an "egg-box" model in the presence of Ca^{2+} [74]. In this design pattern, it is proposed that in a statistical ion-binding process, two polymers are linked in a cooperative manner via Ca^{2+}. However, when focusing on the polyP-driven coacervation process, Ca^{2+} is a vital member of a two-reactant coacervation process alongside polyP [61]. Thereby, Ca^{2+} is not a simple linker but an essential partner pretending a polymer.

5. Conclusion

Due to their similarity to human hard tissue, calcium phosphate nanoparticles have been fabricated, which have qualified as a suitable filler and implant to restore bone defects due to their excellent biocompatibility together with their favorable biodegradability (reviewed in: [45]). Calcium phosphate as a multi-phase scaffold has the tendency to crystallize from the amorphous phase into the different crystalline phases. This property is advantageous for curing bone defects, especially if applied as multiphase calcium phosphate mixtures. Although this property is desirable for this application, it has the disadvantage that the material is only metabolized slowly or not at all in the body [75]. Two results prompted us to investigate the effect of polyP on the stabilization of the amorphous calcium phosphate; first, that β-glycerophosphate can be omitted from the mineralization cocktail used in mineralization studies in vitro, and second, that polyP is a potent inducer of ALP [76]. This enzyme, ALP, is a regulator of bone mineralization and has been implicated in the supply of inorganic phosphate for hydroxyapatite formation [77]. Furthermore, ALP is an enzyme that cleaves polyP [78]. The result is monomeric phosphate, which is an essential and tunable operator for hard tissue/bone formation and resistance of cells to growth stress, and protects against virulence of pathogens [79].

Aside from being an accelerator for the formation of growth promoting and organismic defense metabolites, polyP has two additional and singular properties, first, conversion into the coacervate state and second, the fact that it is the extracellular generator for the supply of ATP to cells. As reported here, oppositely charged (poly)electrolytes such as the polyanionic polyP and Ca^{2+} ions, when mixed in aqueous milieu at neutral pH (pH 7), undergo liquid−liquid phase-separation, coacervation, via cooperative electrostatic interactions. This associative phase separation forms a dense, fluid, polymer-rich phase (the coacervate) and a very electrolytic, aqueous phase. Likewise, and shown here, when the polyanion is added to the Ca^{2+} environment, the coacervate is also obtained at pH 10. Coacervation of polyP and Ca^{2+} is also a process occurring physiologically if the NP synthesized in the cellular acidocalcisomes are transferred to a physiological peptide-containing medium. Since the process of coacervation, as outlined, is not restricted to the extracellular matrix but also occurs intracellularly, it is very likely that also there, the polyP-NP that have been taken up by endocytosis undergo coacervation. As we have described earlier [12], it is the physiologically active form of polyP that enables the cells to embed, protect and, above all, exploit the regeneratively active biomaterial polyP.

The third distinguished feature of polyP is the harvesting of the Gibbs free energy (ΔG) liberated in parallel with the enzymatic cleavage of the energy-rich phosphoanhydride bonds within the polyP chains, leading to ADP formation [21]. From there, this high-energy phosphate metabolite generates ATP during the ADK reaction. The generator-associated enzymes ALP and ADK are present both extra- and intracellularly and enable ATP generation in both compartments. In the extracellular space, ATP is required for extracellular chaperone [80] and kinase activities and intracellularly for feeding anabolic cellular processes and signal transmitters (reviewed in: [21]).

The present study focuses on a modelling approach to shed light on the molecular events during polyP coacervation. The data gathered contribute to a better understanding of the biphasic nature of polyP and the formation of these phases, as well as their physiological roles, the coacervate as the functionally active state and the NP as the extra- and intracellular metabolic energy storage form of this ubiquitous inorganic, but physiological, in all cells present polymer.

Funding

This work was supported by the ERC Advanced Investigator Grant (grant No.: 268476) and three ERC-PoC Grants (Si-Bone-PoC, grant No.: 324564; MorphoVES-PoC, grant No.: 662486; and ArthroDUR, grant No.: 767234). In addition, this work was supported by the International Human Frontier Science Program and the BiomaTiCS research initiative of the University Medical Center, Mainz. Further support came from the BMBF (grant No.: 13GW0403A/B – SKIN-ENERGY) and the BMWi (grant No.: ZF4294002AP9).

Author contributions

W.E.G.M., M.N., I.L, H.C.S. and X.H.W.: Conceptualization, Methodology, Supervision, Formal analysis, Writing – original draft; M.N., I.L and S.F.W.: Visualization, Investigation, Data curation; W.E.G.M., M.N., I.L, S.F.W., H.C.S. and X.H.W.: Funding acquisition and Project administration; W.E.G.M., I.L, H.C.S. and X.H.W.: Resources. All authors read and approved the final manuscript.

Declaration of competing interest

The authors declare that they have no known competing financial interests or personal relationships that could have appeared to influence the work reported in this paper.

Acknowledgements

We thank Mr Michael Plenikowski (modelling; Institute for Physiological Chemistry, University Medical Center of the Johannes Gutenberg University, Mainz) for his extensive contributions. In addition, we are grateful to Mr Gunnar Glasser (SEM; Max Planck Institute for Polymer Research, Mainz) and Ms Dr Maria Kokkinopoulou (TEM; Max Planck Institute for Polymer Research, Mainz) for the very expert electron microscopic examinations.

References

[1] R. Zsigmondy, Zur Erkenntnis der Kolloide: Über irreversible Hydrosole und Ultramikroskopie, G. Fischer, Jena, 1905, p. 185.
[2] I. Langmuir, The constitution and fundamental properties of solids and liquids, J. Am. Chem. Soc. 39 (1917) 1848–1906.
[3] K.B. Blodgett, Monomolecular films of fatty acids on glass, J. Am. Chem. Soc. 56 (1934) 495.

[4] H.G. Bungenberg de Jong, P.H. Teunissen, Negative, nicht amphotere Biokolloide als hochmolekulare Elektrolyte l, Kolloid-Beihefte 47 (1938) 254–320.
[5] N. Strambeanu, L. Demetrovici, D. Dragos, M. Lungu, 1. Nanoparticles: Definition, Classification and General Physical Properties, Springer International Publishing, Basel, 2015, pp. 3–8.
[6] J.J. Verhoef, A.D. Barendrecht, K.F. Nickel, K. Dijkxhoorn, E. Kenne, L. Labberton, O.J. McCarty, R. Schiffelers, H.F. Heijnen, A.P. Hendrickx, H. Schellekens, M.H. Fens, S. de Maat, T. Renné, C. Maas, Polyphosphate nanoparticles on the platelet surface trigger contact system activation, Blood 129 (2017) 1707–1717.
[7] J.I. Weitz, J.C. Fredenburgh, Platelet polyphosphate: the long and the short of it, Blood 129 (2017) 1574–1575.
[8] O. Bütschli, Untersuchungen über Strukturen: insbesondere über Strukturen nichtzelliger Erzeugnisse des Organismus und über ihre Beziehungen zu Strukturen, welche ausserhalb des Organismus entstehen, Wilhelm Engelmann, Leipzig, 1898, p. 411.
[9] J. Esquena, Water-in-water (W/W) emulsions, Curr. Opin. Colloid Interface Sci. 25 (2016) 109–119.
[10] F. Weinbreck, R.H. Tromp, C.G. de Kruif, Composition and structure of whey protein/gum Arabic coacervates, Biomacromolecules 5 (2004) 1437–1445.
[11] H.L. Booij, G. Bungenberg de Jong, Biocolloids and Their Interactions, Springer-Verlag, Vienna, 1956, pp. 8–9.
[12] W.E.G. Müller, S. Wang, E. Tolba, M. Neufurth, M. Ackermann, R. Muñoz-Espí, I. Lieberwirth, G. Glasser, H.C. Schröder, X.H. Wang, Transformation of amorphous polyphosphate nanoparticles into coacervate complexes: an approach for the encapsulation of mesenchymal stem cells, Small 14 (2018), e1801170.
[13] D. Gruber, C. Ruiz-Agudo, H. Cölfen, Cationic coacervates: novel phosphate ionic reservoir for the mineralization of calcium phosphates, ACS Biomater. Sci. Eng. (2022), https://doi.org/10.1021/acsbiomaterials.1c01090.
[14] W.E.G. Müller, E. Tolba, S. Wang, M. Neufurth, I. Lieberwirth, M. Ackermann, H.C. Schröder, X.H. Wang, Nanoparticle-directed and ionically forced polyphosphate coacervation: a versatile and reversible core–shell system for drug delivery, Sci. Rep. 10 (2020), 17147.
[15] X.J. Du, J.L. Wang, S. Iqbal, H.J. Li, Z.T. Cao, Y.C. Wang, J.Z. Du, J. Wang, The effect of surface charge on oral absorption of polymeric nanoparticles, Biomater. Sci. 6 (2018) 642–650.
[16] R. Docampo, W. de Souza, K. Miranda, P. Rohloff, S.N. Moreno, Acidocalcisomes - conserved from bacteria to man, Nat. Rev. Microbiol. 3 (2005) 251–261.
[17] H.-B. Pan, B.W. Darvell, Calcium phosphate solubility: the need for re-evaluation, Cryst. Growth Des. 9 (2009) 639–645.
[18] I. Ramos, F. Gomes, C.M. Koeller, K. Saito, N. Heise, H. Masuda, R. Docampo, W. de Souza, E.A. Machado, K. Miranda, Acidocalcisomes as calcium- and polyphosphate-storage compartments during embryogenesis of the insect Rhodnius prolixus Stahl, PLoS One 6 (2011), e27276.
[19] T. Michigami, Extracellular phosphate as a signaling molecule, Contrib. Nephrol. 180 (2013) 14–24.
[20] A. Formenti, A. De Simoni, E. Arrigoni, M. Martina, Changes in extracellular Ca^{2+} can affect the pattern of discharge in rat thalamic neurons, J. Physiol. 535 (2001) 33–45.
[21] W.E.G. Müller, H.C. Schröder, X.H. Wang, Inorganic polyphosphates as storage for and generator of metabolic energy in the extracellular matrix, Chem. Rev. 119 (2019) 12337–12374.
[22] S. Tatur, N. Groulx, S.N. Orlov, R. Grygorczyk, Ca^{2+}-dependent ATP release from A549 cells involves synergistic autocrine stimulation by coreleased uridine nucleotides, J. Physiol. 584 (2007) 419–435.
[23] W.E.G. Müller, E. Tolba, H.C. Schröder, S. Wang, G. Glaßer, R. Muñoz-Espí, T. Link, X.H. Wang, A new polyphosphate calcium material with morphogenetic activity, Mater. Lett. 148 (2015) 163–166.
[24] W.E.G. Müller, S. Wang, M. Wiens, M. Neufurth, M. Ackermann, D. Relkovic, M. Kokkinopoulou, Q.L. Feng, H.C. Schröder, X.H. Wang, Uptake of polyphosphate microparticles in vitro (SaOS-2 and HUVEC cells) followed by an increase of the intracellular ATP pool size, PLoS One 12 (12) (2017), e0188977.
[25] H.M. Berman, J. Westbrook, Z. Feng, G. Gilliland, T.N. Bhat, H. Weissig, I.N. Shindyalov, P.E. Bourne, The protein data bank, Nucleic Acids Res. 28 (2000) 235–242.
[26] G. Raffaini, Surface chemistry, crystal structure, size and topography role in the albumin adsorption process on TiO_2 anatase crystallographic faces and its 3D-nanocrystal: a molecular dynamics study, Coatings 11 (2021) 420.
[27] E. Tolba, X.H. Wang, M. Ackermann, M. Neufurth, R. Muñoz-Espí, H.C. Schröder, W.E.G. Müller, In situ polyphosphate nanoparticle formation in hybrid poly(vinyl alcohol)/karaya gum hydrogels: a porous scaffold inducing infiltration of mesenchymal stem cells, Adv. Sci. 6 (2019), 1801452.
[28] W.E.G. Müller, R.K. Zahn, Metabolism of 1-ß-D-arabinofuranosyluracil in mouse L5178y cells, Cancer Res. 39 (1979) 1102–1107.
[29] W.E.G. Müller, M. Neufurth, S.F. Wang, R.W. Tan, H.C. Schröder, X.H. Wang, Morphogenetic (mucin expression) as well as potential anti-corona viral activity of the marine secondary metabolite polyphosphate on A549 cells, Mar. Drugs 18 (2020) 639.
[30] H. Yan, M.D. Tsai, Nucleoside monophosphate kinases: structure, mechanism, and substrate specificity, Adv. Enzymol. Relat. Area Mol. Biol. 73 (1999) 103–134.
[31] T. Friis, A.M. Engel, C.D. Bendiksen, L.S. Larsen, G. Houen, Influence of levamisole and other angiogenesis inhibitors on angiogenesis and endothelial cell morphology in vitro, Cancers 5 (2013) 762–785.
[32] R. Petrucci, F. Herring, J. Madura, C. Bissonnette, General Chemistry: Principles and Modern Applications, eleventh ed., Prentice-Hall, NJ, 2022. Upper Saddle River.
[33] A. Khoshmanesh, P.L. Cook, B.R. Wood, Quantitative determination of polyphosphate in sediments using Attenuated Total Reflectance-Fourier Transform Infrared (ATR-FTIR) spectroscopy and partial least squares regression, Analyst 137 (2012) 3704–3709.
[34] D.M. Pickup, R.J. Newport, E.R. Barney, J.Y. Kim, S.P. Valappil, J.C. Knowles, Characterisation of phosphate coacervates for potential biomedical applications, J. Biomater. Appl. 28 (2014) 1226–1234.
[35] A. Michelmore, W. Gong, P. Jenkins, J. Ralston, The interaction of linear polyphosphates with titanium dioxide surfaces, Phys. Chem. Chem. Phys. 2 (2000) 2985–2992.
[36] P.Y. Shih, J.Y. Ding, S.Y. Lee, ^{31}P MAS-NMR and FTIR analyses on the structure of CuO-containing sodium poly- and meta-phosphate glasses, Mater. Chem. Phys. 80 (2003) 391–396.
[37] A. Momeni, M.J. Filiaggi, Rheology of polyphosphate coacervates, J. Rheol. 60 (2016) 25.
[38] T. Lu, E. Spruijt, Multiphase complex coacervate droplets, J. Am. Chem. Soc. 142 (2020) 2905–2914.
[39] A. Chatterjee, J. Higham, R.H. Henchman, Instantaneous, parameter-free methods to define a solute's hydration shell, J. Chem. Phys. 143 (2015), 234501.
[40] G. Pálinkás, K. Heinzinger, Hydration shell structure of the calcium ion, J. Mol. Liq. 274 (2019) 261–269.
[41] M. Shimabukuro, Antibacterial property and biocompatibility of silver, copper, and zinc in titanium dioxide layers incorporated by one-step micro-arc oxidation: a review, Antibiotics (Basel) 9 (2020) 716.
[42] G. Leyhausen, B. Lorenz, H. Zhu, W. Geurtsen, R. Bohnensack, W.E.G. Müller, H.C. Schröder, Inorganic polyphosphate in human osteoblast-like cells, J. Bone Miner. Res. 13 (1998) 803–812.
[43] W.E.G. Müller, S.I. Belikov, W. Tremel, C.C. Perry, W.W.C. Gieskes, A. Boreiko, H.C. Schröder, Siliceous spicules in marine demosponges (example Suberites domuncula), Micron 37 (2006) 107–120.
[44] H.C. Schröder, X.H. Wang, W. Tremel, H. Ushijima, W.E.G. Müller, Biofabrication of biosilica-glass by living organisms, Nat. Prod. Rep. 25 (2008) 455–474.
[45] V. Sokolova, M. Epple, Biological and medical applications of calcium phosphate nanoparticles, Chemistry 27 (2021) 7471–7488.
[46] X.H. Wang, H.C. Schröder, W.E.G. Müller, Amorphous polyphosphate, a smart bioinspired nano-/bio-material for bone and cartilage regeneration: towards a new paradigm in tissue engineering, J. Math. Chem. B 6 (2018) 2385–2412.
[47] F. Müller, N.J. Mutch, W.A. Schenk, S.A. Smith, L. Esterl, H.M. Spronk, S. Schmidbauer, W.A. Gahl, J.H. Morrissey, T. Renné, Platelet polyphosphates are proinflammatory and procoagulant mediators in vivo, Cell 139 (2009) 1143–1156.
[48] B.F. Kraemer, M. Geimer, M. Franz-Wachtel, T. Lamkemeyer, H. Mannell, S. Lindemann, Extracellular matrix-specific platelet activation leads to a differential translational response and protein de novo synthesis in human platelets, Int. J. Mol. Sci. 21 (2020) 8155.
[49] S. Lickert, K. Selcuk, M. Kenny, J.L. Mehl, S.M. Früh, M.A. Burkhardt, J.D. Studt, I. Schoen, V. Vogel, Platelets Exploit Fibrillar Adhesions to Assemble Fibronectin Matrix Revealing New Force-Regulated Thrombus Remodeling Mechanisms, bioRxiv, 2020, https://doi.org/10.1101/2020.04.20.050708.
[50] S.A. Smith, N.J. Mutch, D. Baskar, P. Rohloff, R. Docampo, J.H. Morrissey, Polyphosphate modulates blood coagulation and fibrinolysis, Proc. Natl. Acad. Sci. USA 103 (2006) 903–908.
[51] J. Roewe, G. Stavrides, M. Strueve, A. Sharma, F. Marini, A. Mann, S.A. Smith, Z. Kaya, B. Strobl, M. Mueller, C. Reinhardt, J.H. Morrissey, M. Bosmann, Bacterial polyphosphates interfere with the innate host defense to infection, Nat. Commun. 11 (2020) 4035.
[52] A. Di Daniele, Y. Antonucci, S. Campello, Migrasomes, new vescicles as Hansel and Gretel white pebbles? Biol. Direct 17 (2022) 8.
[53] Y. Zhang, W. Guo, M. Bi, W. Liu, L. Zhou, H. Liu, F. Yan, L. Guan, J. Zhang, J. Xu, Migrasomes: From biogenesis, release, uptake, rupture to homeostasis and diseases, Oxid. Med. Cell. Longev. 2022 (2022) 4525778.
[54] M.R. Thomas, E.K. O'Shea, An intracellular phosphate buffer filters transient fluctuations in extracellular phosphate levels, Proc. Natl. Acad. Sci. USA 102 (2005) 9565–9570.
[55] M.E. Solesio, L.C. Garcia Del Molino, P.A. Elustondo, C. Diao, J.C. Chang, E.V. Pavlov, Inorganic polyphosphate is required for sustained free mitochondrial calcium elevation, following calcium uptake, Cell Calcium 86 (2020), 102127.
[56] H. Schepler, X.H. Wang, M. Neufurth, S. Wang, H.C. Schröder, W.E.G. Müller, The therapeutic potential of inorganic polyphosphate: a versatile physiological polymer to control coronavirus disease (COVID-19), Theranostics 11 (2021) 6193–6213.
[57] H. Schepler, M. Neufurth, S.F. Wang, Z.D. She, H.C. Schröder, X.H. Wang, W.E.G. Müller, Acceleration of chronic wound healing by bio-inorganic polyphosphate: in vitro studies and first clinical applications, Theranostics 12 (2022) 18–34.
[58] M.C. Groeneveld, T. Van den Bos, V. Everts, W. Beertsen, Cell-bound and extracellular matrix-associated alkaline phosphatase activity in rat periodontal ligament, Experimental Oral Biology Group. J. Periodontal Res. 31 (1996) 73–79.
[59] W.E.G. Müller, M. Ackermann, E. Tolba, M. Neufurth, I. Ivetac, M. Kokkinopoulou, H.C. Schröder, X.H. Wang, Role of ATP during the initiation of microvascularization. Acceleration of an autocrine sensing mechanism facilitating chemotaxis by inorganic polyphosphate, Biochem. J. 475 (2018) 3255–3273.
[60] W.M. Aumiller Jr., C.D. Keating, Phosphorylation-mediated RNA/peptide complex coacervation as a model for intracellular liquid organelles, Nat. Chem. 8 (2016) 129–137.
[61] D.F. Franco, H.G. De Oliveira Barud, H.S. Barud, O.B. Oliveira, A.B. Meneguin, L.F. de Oliveira, M.A.P. Silva, S.J.L. Ribeiro, M. Nalin, A review on polyphosphate coacervates-structural properties and bioapplications, J. Sol. Gel Sci. Technol. 94 (2020) 531–554.

[62] D. Priftis, N. Laugel, M. Tirrell, Thermodynamic characterization of polypeptide complex coacervation, Langmuir 28 (2012) 15947–15957.
[63] D.A. Scott, R. Docampo, J.A. Dvorak, S. Shi, R.D. Leapman, In situ compositional analysis of acidocalcisomes in *Trypanosoma cruzi*, J. Biol. Chem. 272 (1997) 28020–28029.
[64] X.H. Wang, M. Ackermann, E. Tolba, M. Neufurth, F. Wurm, Q.L. Feng, S.F. Wang, H.C. Schröder, W.E.G. Müller, Artificial cartilage bio-matrix formed of hyaluronic acid and Mg^{2+}-polyphosphate, Eur. Cell. Mater. 32 (2016) 271–283.
[65] W.E.G. Müller, M. Ackermann, B. Al-Nawas, L.A.R. Righesso, R. Muñoz-Espí, E. Tolba, M. Neufurth, H.C. Schröder, X.H. Wang, Amplified morphogenetic and bone forming activity of amorphous versus crystalline calcium phosphate/polyphosphate, Acta Biomater. 118 (2020) 233–247.
[66] A. Momeni, M.J. Filiaggi, Comprehensive study of the chelation and coacervation of alkaline earth metals in the presence of sodium polyphosphate solution, Langmuir 30 (2014) 5256–5266.
[67] A. Kornberg, Inorganic polyphosphate: toward making a forgotten polymer unforgettable, J. Bacteriol. 177 (1995) 491–496.
[68] Inorganic polyphosphates; biochemistry, biology, biotechnology, in: H.C. Schröder, W.E.G. Müller (Eds.), Progress in Molecular and Subcellular Biology, vol. 23, Springer-Verlag, Berlin, 1999.
[69] I.S. Kulaev, V. Vagabov, T. Kulakovskaya, The Biochemistry of Inorganic Polyphosphates, second ed., John Wiley, Chichester, 2004.
[70] W.E.G. Müller, S. Wang, M. Neufurth, M. Kokkinopoulou, Q.L. Feng, H.C. Schröder, X.H. Wang, Polyphosphate as a donor of high-energy phosphate for the synthesis of ADP and ATP, J. Cell Sci. 130 (2017) 2747–2756.
[71] W.E.G. Müller, E. Tolba, Q.L. Feng, H.C. Schröder, J.S. Markl, M. Kokkinopoulou, X.H. Wang, Amorphous Ca^{2+} polyphosphate nanoparticles regulate ATP level in bone-like SaOS-2 cells, J. Cell Sci. 128 (2015) 2202–2207.
[72] I. Mäger, K. Langel, T. Lehto, E. Eiríksdóttir, U. Langel, The role of endocytosis on the uptake kinetics of luciferin-conjugated cell-penetrating peptides, Biochim. Biophys. Acta 1818 (2012) 502–511.
[73] E. Kizilay, A.B. Kayitmazer, P.L. Dubin, Complexation and coacervation of polyelectrolytes with oppositely charged colloids, Adv. Colloid Interface Sci. 167 (2011) 24–37.
[74] E. Morris, P. Smith, D. Rees, Biological interactions between polysaccharides and divalent cations: the egg-box model, FEBS Lett. 32 (1973) 195–198.
[75] F.C. Meldrum, H. Cölfen, Controlling mineral morphologies and structures in biological and synthetic systems, Chem. Rev. 108 (2008) 4332–4432.
[76] W.E.G. Müller, X.H. Wang, B. Diehl-Seifert, K. Kropf, U. Schloßmacher, I. Lieberwirth, G. Glasser, M. Wiens, H.C. Schröder, Inorganic polymeric phosphate/polyphosphate as an inducer of alkaline phosphatase and a modulator of intracellular Ca^{2+} level in osteoblasts (SaOS-2 cells) in vitro, Acta Biomater. 7 (2011) 2661–2671.
[77] P. Szulc, D.C. Bauer, Biochemical markers of bone turnover, in: R. Marcus, D. Dempster, J. Cauley, D. Feldman (Eds.), Osteoporosis, fourth ed., Elsevier/Academic Press, Cambridge (MA), 2013, pp. 1573–1610.
[78] B. Lorenz, H.C. Schröder, Mammalian intestinal alkaline phosphatase acts as highly active exopolyphosphatase, Biochim. Biophys. Acta 1547 (2001) 254–261.
[79] N.N. Rao, M.R. Gómez-García, A. Kornberg, Inorganic polyphosphate: essential for growth and survival, Annu. Rev. Biochem. 78 (2009) 605–647.
[80] L. Xie, U. Jakob, Inorganic polyphosphate, a multifunctional polyanionic protein scaffold, J. Biol. Chem. 294 (2019) 2180–2190.